EFDA–JET–CP(14)01/36

A. Kirschner, D. Matveev, D. Borodin, M. Airila, S. Brezinsek, M. Groth,
S. Wiesen, A. Widdowson, J. Beal, H.G. Esser, J. Likonen, N. Bekris,
R. Ding and JET EFDA contributors

Modelling of the Material Transport and Layer Formation in the Divertor of JET: Comparison of ITER-Like Wall with Full Carbon Wall Conditions

Modelling of the Material Transport and Layer Formation in the Divertor of JET: Comparison of ITER-Like Wall with Full Carbon Wall Conditions

A. Kirschner[1], D. Matveev[1], D. Borodin[1], M. Airila[2], S. Brezinsek[1], M. Groth[3], S. Wiesen[1], A. Widdowson[4], J. Beal[5], H.G. Esser[1], J. Likonen[2], N. Bekris[6], R. Ding[7] and JET EFDA contributors*

JET-EFDA, Culham Science Centre, OX14 3DB, Abingdon, UK

[1]Institute of Energy and Climate Research – Plasma Physics, Forschungszentrum Jülich GmbH, Trilateral Euregio Cluster, 52425 Jülich, Germany
[2]VTT Technical Research Centre of Finland, 02044 VTT, Finland
[3]Aalto University, Otakaari 4, 02015 Espoo, Finland
[4]Culham Centre for Fusion Energy, Abingdon OX14 3DB, UK
[5]York Plasma Institute, Department of Physics, University of York, Heslington, York, YO10 5DD, UK
[6]Karlsruhe Institute of Technology, Institute for Technical Physics, Hermann-von-Helmholtz-Platz 1, Bau 451, 76344 Eggenstein-Leopoldshafen, Germany
[7]Institute of Plasma Physics, Chinese Academy of Sciences, P.O. Box 1126, Hefei, Anhui 230031, P.R.China
** See annex of F. Romanelli et al, "Overview of JET Results", (24th IAEA Fusion Energy Conference, San Diego, USA (2012)).*

Preprint of Paper to be submitted for publication in Proceedings of the
21st International Conference on Plasma Surface Interactions, Kanazawa, Japan
26th May 2014 – 30th May 2014

ABSTRACT

Impurity transport within the inner JET divertor has been modelled with ERO to estimate the transport to and the resulting deposition at remote areas. Various parametric studies involving divertor plasma conditions and strike point position have been performed. In JET-ILW (beryllium main chamber and tungsten divertor) beryllium, flowing from the main chamber into the divertor and then effectively reflected at the tungsten divertor tiles, is transported to remote areas. The tungsten flux to remote areas in L-Mode is in comparison to the beryllium flux negligible due to small sputtering. However, tungsten is sputtered during ELMs in H-Mode conditions. Nevertheless, depending on the plasma conditions, strike point position and the location of the remote area, the maximum resulting tungsten flux to remote areas is at least ~ 3 times lower than the corresponding beryllium flux. Modelled beryllium and tungsten deposition on a rotating collector probe located below tile 5 is in good agreement with measurements if the beryllium influx into the inner divertor is assumed to be in the range of 0.1% relative to the deuterium ion flux and erosion due to fast charge exchange neutrals is considered. Comparison between JET-ILW and JET-C is presented.

1. INTRODUCTION

The erosion of first wall material in fusion devices leads to life time limitations of plasma facing components. In addition, the eroded particles will be deposited somewhere within the device together with the co-deposition of radioactive tritium. Due to safety reasons the overall amount of retained tritium within the wall surfaces is limited, which therefore could lead to restricted availability of future devices such as ITER. The possible retention of tritium at remote areas of the vacuum vessel, which are not in direct line-of-sight from the plasma, is particularly critical as cleaning of such areas is very difficult. Predictions of tritium retention for future fusion devices including deposition on remote areas are therefore important. Such estimations are normally based on the scaling of experimental data from present devices in combination with modelling [1, 2]. In order to test their capability, it is essential to benchmark the modelling tools against experimental results. For such benchmarking, the JET device with the ITER-like wall (JET-ILW) is the most suitable existing experiment since it is operating with beryllium main wall and tungsten divertor as it is foreseen to be the case in ITER [3, 4].

The present contribution is about the modelling of impurity transport within the inner divertor of JET-ILW including the erosion of the tungsten divertor tiles and the resulting layer deposition. For this purpose the three-dimensional Monte-Carlo code ERO [5] has been applied. Estimations of beryllium and tungsten particle fluxes to the remote areas – in particular the louvre region and the area below the semi-horizontal outer target plate (tile 5) – will be given as well as the corresponding deposition rates. At present, some measured, campaign-integrated deposition data at these locations in JET-ILW are available but there is no shot-resolved information from the Quartz Micro Balances (QMB) except of a few data from the restart phases. However, a first comparison of the modelling results with the beryllium and tungsten deposition measurements provided by the rotating collector probe located below tile 5 will be given. Modelling of carbon fluxes to the remote areas of the inner divertor for full carbon wall conditions in JET-C will be shown and will be compared to the JET-ILW

results. The influence of various parameters such as strike point position and plasma parameters (L-Mode and H-Mode) will also be studied. Finally, based on the modelling and on experimental observations, conclusions related to the impurity influx to the inner divertor for both configurations (JET-ILW and JET-C) will be drawn and discussed in relation to the first wall replacement, i.e. changing from full carbon to ILW conditions [6].

2. MODELLING OF IMPURITY TRANSPORT IN THE INNER DIVERTOR OF JET

2.1. REFLECTION AND SPUTTERING DATA

Species from the background plasma (deuterium and impurities) are normally not followed within the ERO simulations. Therefore, reflection coefficients and sputter yields for background species are pre-calculated with the TRIM [7] code for a set of impact energies and angles. However, to determine the erosion due to these particles and the reflection of these particles, the distribution of their impact energy and angle has to be known. Whereas ERO essentially can calculate these distributions by injection of background particles far away from the surface and following them until reaching the surface [8], the present work applies a simplified approach. The mean angle of incidence for background deuterium ions D^+, beryllium Be^{2+} and carbon C^{2+} ions is assumed to be 60°. This is in good agreement with earlier ERO runs [8], analytical calculations [9] and also particle-in-cell results [10] for typical conditions within the divertor of fusion devices at shallow magnetic field angle relative to the surface. The mean impact energy of an ion with charge state Z is assumed to be $3ZT_e + 2T_i$, which considers acceleration in the sheath potential $3T_e$. The energy of reflected particles is set by TRIM whereas the energy of sputtered species is given by a Thompson distribution around half the binding energy of the sputtered material [11], which is typically in good agreement with TRIM results. The angle of both reflected and sputtered species is given by a cosine distribution relative to the surface normal. It has to be noted that the surfaces of the W-coated CFC tiles of JET-ILW have a rather large roughness of about 5μm [12], which also could change with exposure time. Thus, the effective reflection coefficient and sputtering yield will be affected by the surface roughness, see e.g. reference [13] demonstrating increased deposition, and thus effectively reduced reflection with rough surfaces compared to smooth ones. Within the present work such effects are not considered as we were mainly focused on the general trends of particle fluxes to the remote areas of the JET divertor. As the impact energy and angle of test particles followed in ERO are known, the corresponding reflection coefficients and sputtering yields can be calculated straight forward.

The TRIM calculations show that tungsten sputtering by deuterium is negligible at small impact energies. Only at energies larger than around 500eV, which can appear during ELMs, sputtering yields in the percent range are reached. However, such sputter yields of tungsten occur for beryllium impact already at energies around 70eV. Reflection of beryllium on tungsten is very effective and larger than 50% at impact energies higher than ~ 5eV reaching maximal reflection of about 90% at impact energy of 20eV. Maximum reflection of carbon on carbon with about 20% occurs at impact energies around 200eV.

2.2. Input parameter for the ERO modelling

To study the impurity transport to remote areas of the inner divertor in dependence on strike point (SP) position and plasma conditions the following assumptions are made: the magnetic field is fixed to 2.5T and within the flux surfaces electron density (n_e) and electron and ion temperature (T_e, T_i) are constant. The values of n_e, T_e and T_i within the separatrix and thus also at the strike point are given as input parameters. An exponential decay with decay lengths λ of the plasma parameters perpendicular to the separatrix towards the scrape-off layer (SOL) and towards the private flux region (PFR) is assumed. The plasma parameters are assumed to be constant in toroidal direction.

According to Langmuir probe measurements of a typical L-Mode discharge (from JET-C operation) [14] the following parameters are deduced for the inner divertor: T_e(SP) = 10eV, n_e(SP) = 1e13cm^{-3}, $\lambda_{n,SOL}$ = 27mm, $\lambda_{T,SOL}$ = 110mm, $\lambda_{n,PFR}$ = 16mm and $\lambda_{T,PFR}$ = 25mm. The ion temperature T_i is assumed to be equal the electron temperature T_e. H-Mode conditions are simulated in a simplified way by assuming increased temperature (800eV within separatrix) and density (5e13cm^{-3} within separatrix) during the ELMs and L-Mode conditions for the inter-ELM phases. The intra-ELM parameters are chosen as upper limit. During the ELM phases either the same decay lengths as for L-Mode are assumed or alternatively, according to [15], twice reduced values. The inner strike point is located either on the lower vertical tile 3 or on the horizontal tile 4. Figure 1 shows the divertor tile geometry together with the simulation volume used in the ERO simulations.

The ERO simulations presented here are limited to the region of the inner divertor. Therefore, the amount of impurities flowing into the divertor, originating mainly from main wall erosion, has to be defined by input parameters. To begin with it is assumed that 1% Be^{2+} for JET-ILW and 1% C^{2+} for JET-C relative to the incoming deuterium ion flux is entering the inner divertor. The reasonability and conclusions drawn from these assumptions will be discussed in section 2.3.3. We exclude any beryllium flux for JET-C and any carbon flux for JET-ILW, which is in agreement with observations after replacing the carbon divertor with a tungsten one [6].

2.3. EROSION AND DEPOSITION ALONG INNER DIVERTOR TILES

2.3.1. JET-ILW with L-Mode conditions

The simulations are performed with pure tungsten tiles without the consideration of material mixing of tungsten and beryllium – possible effects from material mixing will be briefly addressed in section 3. First of all the inner strike point is located on the vertical tile 3 at z = 90mm; in figure 2 the separatrix is indicated with a solid line. Figure 2 shows exemplarily the distribution of sputtered tungsten atoms W^0 and the resulting ions W^+ as well as the reflected beryllium atoms Be^0 and the resulting ions Be^+ within a poloidal cross section of the inner divertor (i.e. integrated over the toroidal direction). Resulting profiles of reflected beryllium, eroded tungsten and deposition along the divertor tiles are summarised in figure 3. The x-axis gives the number of surface cell used in the ERO simulation, starting at the top part of tile 3 (z = 180mm) with #cell = 0. It is seen that the amount of tungsten sputtering is very small compared to the beryllium reflection flux, at the strike point a factor of about 500 smaller. Tungsten under L-Mode conditions is only sputtered by

beryllium as the threshold energy for deuterium ions is larger than their impact energy. About 87% of sputtered tungsten and about 41% of reflected beryllium is deposited on the inner target tiles. With the strike point located on tile 3 at z = 90mm, main loss of sputtered tungsten particles not deposited takes place in the +x direction (~ 10%). Beryllium not deposited leaves the simulation volume mainly in +x and +z direction (~ 55%).

Moving the strike point upwards by 50mm along tile 3 to z = 140mm decreases the overall amount of deposition (84% for tungsten and 27% for beryllium) on the inner tiles. The number of particles leaving the simulation volume in +z direction increases accordingly. Finally, putting the inner strike point onto the sloping part of tile 4, leads to 65% tungsten and 40% beryllium deposition on the inner tile surfaces. Under this configuration main loss of particles takes place into the direction of the inner louvre (opening between tile 3 and tile 4): 33% of sputtered tungsten and 41% of reflected beryllium escapes to this area. The resulting profiles of particle reflection, erosion and deposition for L-Mode conditions and strike point located on the sloping part of tile 4 are presented in figure 4.

The simulation results discussed so far did not include tungsten sputtering by followed test particles, thus in particular self-sputtering has not been considered. Taking this into account increases the overall amount of tungsten sputtering by a factor of about two; however, the tungsten flux is still much smaller than the beryllium flux from reflection. There is still more than two orders of magnitude difference between these two particle fluxes.

2.3.2. JET-ILW for ELM conditions

Setting the strike point on tile 3 at z = 90mm and assuming the plasma parameters from the ELM-phase, $T_e(SP)$ = 800eV, $n_e(SP)$ = 5e13cm^{-3} and same decay lengths as for L-Mode conditions, results now in significant tungsten erosion by deuterium and beryllium, which is even larger than the beryllium reflection flux. The deposition fraction of tungsten on the inner divertor tiles increases to ~ 95% compared to 87% in L-Mode due to the higher electron density and temperature. On the other hand, the amount of beryllium deposition decreases to ~ 30% (compared to 41% in L-Mode) due to larger energy of the reflected beryllium, whereby more beryllium atoms can leave the simulation volume in +x and +z direction.

Changing the strike point position under ELM conditions from tile 3 to the sloping part of tile 4 does not significantly influence the overall amounts of deposition for tungsten and beryllium on the tiles. As for L-Mode conditions, main loss of particles is now due to transport to the louvre area.

According to [15] the power decay length for ELMs is about two times smaller than for L-Mode conditions. To study the influence of varying decay lengths for electron density and temperature during an ELM, these values have been halved with respect to the so-far used L-Mode decay lengths: $\lambda_{n,SOL}$ = 27/2mm, $\lambda_{T,SOL}$ = 110/2mm, $\lambda_{n,PFR}$ = 16/2mm and $\lambda_{T,PFR}$ = 25/2mm. According ERO simulations have been done on the example of the case with the strike point positioned on tile 3 (z = 90mm). With halved decay lengths the overall fraction of deposition along the tiles is nearly unchanged for beryllium and tungsten. However, the absolute fluxes are reduced by a factor of about 2 due to reduced temperature and density within the SOL and PFR.

The above-described simulations for the ELM phase do not include sputtering by followed test particles. Similar to L-Mode conditions, including this additional sputtering channel roughly doubles the overall amount of tungsten sputtering within an ELM.

Spectroscopic measurements of the tungsten gross sputtering at the outer divertor of JET-ILW [16] indicate that the sputtered tungsten flux during ELM-phase is about 1000 times larger than during inter-ELM phase (with electron temperature larger than 30eV), if an ELM duration of 500µs is assumed. The present modelling for the inner divertor reveals an according factor of about 40.000 if the reduced decay lengths for electron density and temperature are assumed. Without reduced decay lengths the factor increases to about 80.000. Both modelling and measurement clearly show that tungsten sputtering is dominated by the intra-ELM phase. In the modelling this dominance is much more pronounced than measured because L-Mode conditions have been assumed for the inter-ELM phase. A similar factor between intra- and inter-ELM tungsten sputtering as measured would be achieved in the modelling if larger electron temperature and/or density would be assumed for the inter-ELM conditions (e.g. temperature larger than 30eV at the strike point instead of 10eV assumed so far).

2.3.3. Impurity flux to remote areas and resulting deposition

The fluxes of beryllium and tungsten to the remote areas of the inner divertor of JET have been calculated from the above-described ERO simulations. Figure 1 illustrates the ERO simulation volume together with the boundary surfaces to the inner louvre region and to the region below tile 5. Figure 5 summarises the estimated fluxes for JET-ILW given in particles per second and related to the full toroidal circumference of JET. The data for the strike point on tile 3 correspond to strike point position z = 90mm. For H-Mode conditions in JET-C it is assumed that the ELM has a length of 200µs and a frequency of 50Hz. The particle fluxes during H-Mode are therefore given by $\Gamma_{\text{H-Mode}} = 1/100 \cdot \Gamma_{\text{ELM}} + 99/100 \cdot \Gamma_{\text{L-Mode}}$ supposing L-Mode conditions for the inter-ELM phases. It has been found that the ELM length in JET-ILW is significantly larger than in JET-C. An average value of 500µs leads to the following H-Mode particle fluxes in JET-ILW: $\Gamma_{\text{H-Mode}} = 1/40 \cdot \Gamma_{\text{ELM}} + 39/40 \cdot \Gamma_{\text{L-Mode}}$. Compared to L-Mode parameters, halved decay lengths for density and temperature are used for ELM conditions. The simulations reveal that only neutral beryllium and tungsten particles are able to reach the remote area below the tile 5 whereas also ions can enter the louvre region. It is seen that in general the fluxes to the louvre area are larger with strike point on tile 4 whereas larger fluxes to the tile 5 area are obtained with strike point on tile 3. Similar tendencies have been observed experimentally by means of shot-resolved QMB measurements performed under JET-C conditions for carbon [17, 18] and modelled earlier with the ERO code [19, 20]. For L-Mode conditions the tungsten fluxes are much smaller than the beryllium fluxes. Significant amount of tungsten is transported to the louvre region during H-Mode; however, the tungsten flux to the tile 5 area during H-Mode is still very small compared to the corresponding beryllium flux. The beryllium flux to the remote areas under H-Mode conditions is up to 1.5 times larger than under L-Mode. Shifting the strike point on tile 3 upwards by 50mm within L-Mode conditions reduces

the beryllium and tungsten fluxes to the remote areas. In particular, no tungsten is able to enter the louvre area and also the beryllium flux to this region is reduced by a factor of ~ 20. The fluxes to the area below tile 5 are reduced by factors of ~ 5 for tungsten and ~ 2 for beryllium. Assuming the decay lengths for density and temperature from L-Mode also for ELM conditions (instead of halved values) leads to increased particles fluxes to the louvre area of a factor between 1.1 and 5, the latter one in case of tungsten and strike point on tile 3. Also the beryllium fluxes to the area below tile 5 slightly increase (factor ~ 1.3) but the tungsten flux decreases (factor 2 for strike point on tile 4 and factor 7 for strike point on tile 3).

Beryllium and tungsten deposition after the first JET-ILW campaign have been measured amongst others [21] on the rotating collector probe (RC) below tile 5 by means of Nuclear Reaction Analysis [22]. The measured beryllium varies between 2e16 and 8e16 Be/cm^2, while tungsten deposition is around 5e14 W/cm^2. However, the measured tungsten deposition is very small and therefore has considerable uncertainty. The measurement points on the RC typically correspond to about 50 discharges, excluding invalid discharges. Assuming 20s of divertor phase per pulse then results in deposition rates of 2e13 – 8e13 Be/(cm^{2}s) and 5e11 W/(cm^{2}s). It has to be noted that the 50 pulses also include some limiter discharges, where less material transport to the remote areas can be expected. Therefore, the estimated deposition rates per second can be interpreted as lower values.

The ERO simulations only deliver the impurity fluxes to the remote areas as discussed before. However, taking these results as input for 3D-GAPS [23] simulations, we obtain deposition rates, which can be directly compared with the measurements. Within 3D-GAPS the incoming particles are followed considering the detailed geometry of the remote area below the tile 5 and reflection within it. For the reflection it is assumed that the surfaces within the remote area are covered with beryllium and corresponding reflection coefficients from TRIM simulations are applied. Eventually, part of the entering particles is deposited on the RC. Possible erosion of deposited particles from the RC is not included. Table 1 summarises the modelled and measured deposition rates.

It can be seen that the modelled beryllium deposition applying L-Mode conditions is by a factor of 5 to 100 too large. Shifting the strike point upwards on tile 3 within L-Mode would decrease the modelled deposition by a factor of ~ 2 and accordingly the difference between modelled and measured beryllium deposition decreases. H-Mode conditions, applying half decay lengths for density and temperature, increases the beryllium deposition leading to deposition on the RC which is now 5 – 150 times larger than measured.

Tungsten deposition from the modelling yields maximum deposition rates on the RC of about 5e13 W/(cm^{2}s) and thus a factor of 100 larger than the averaged measured tungsten deposition. This modelled upper value corresponds to the case of maximum tungsten flux entering into the tile 5 region, which occurs in ERO during H-Mode with half decay lengths for density and temperature during ELM phase and strike point on tile 3. The modelled tungsten deposition on the RC during L-Mode conditions is at least a factor of 60 smaller than the one from H-Mode. Anyhow, a quantitative comparison between modelling and experiment is very difficult due to the rather large uncertainties in the measured tungsten deposition.

Once again it has to be noted that the ERO simulations assumed an incoming beryllium flux to the divertor of 1% relative to the incoming deuterium ion flux. Taking the same assumption for the carbon influx under JET-C conditions, results in remote fluxes of carbon as shown in figure 6. Chemical erosion of carbon by means of methane formation has been considered with a yield of 1%. Reflection for neutral hydrocarbons is set to 100% and for ionised ones to 10%. Enhanced re-erosion of re-deposited carbon is not considered here but has been studied in [20] within the modelling of deposition on the QMB below tile 5 – the extreme assumption of 10 times enhanced chemical and physical sputtering for re-deposits increased the deposition on the QMB by a factor of about 2. The modelled remote carbon fluxes for JET-C within the present work are not very different from the according beryllium fluxes for JET-ILW shown in figure 5 except for the fluxes to the inner louvre with strike point located on tile 3: for this case the carbon flux is three times larger for L-Mode and even 9 times larger for H-Mode compared to the beryllium flux.

However, there are many experimental observations suggesting that the beryllium influx into the inner divertor within JET-ILW is significantly smaller than the according carbon influx in JET-C. For instance, erosion estimations for JET-ILW indicate that the beryllium source from the main wall erosion is about 5 times smaller than the according carbon source in JET-C. Monitoring shots in JET-ILW indicate a beryllium concentration in the inner divertor plasma (deduced from spectroscopy) of about 0.2% Be [6], whereas the carbon concentration for similar plasma conditions is 5 to 10 times larger. Also, first estimations of the overall beryllium deposition within the inner divertor of JET-ILW shows significantly reduced deposition rates compared to carbon in JET-C. For example, the carbon deposition rate from JET-C measured on the RC below the tile 5 [24] is in average 5 – 10 times larger than the beryllium deposition rate from JET-ILW on that RC. Finally, modelling with WALLDYN for JET-ILW results in beryllium fluxes entering the inner divertor, which are in the order of 0.1% near the inner strike point [25]. Whereas the assumption for the carbon influx into the inner divertor of JET-C being in the order of 1% seems to be reasonable, the beryllium influx for JET-ILW could be 5 to 10 times smaller. Such reduction would accordingly decrease the modelled beryllium deposition at the RC and leading to values, which are in the same order of magnitude as the measurements. Moreover, possible erosion due to fast CX neutrals (not included in the modelling) would further reduce the modelled values. QMB measurements with JET-C have shown that even net erosion takes place within the remote regions under certain conditions (e.g. QMB below tile 5 shows net erosion if the strike point is located on the sloping part of tile 4 [17]). This can be explained by chemical erosion of carbon although physical sputtering due to fast CX neutrals cannot be excluded.

3. SUMMARY AND CONCLUSIONS

ERO modelling of the impurity fluxes to the remote areas of the inner divertor of JET-ILW has shown that:

- Significant tungsten fluxes only occur during H-Mode discharges. Self-sputtering typically doubles the overall tungsten erosion within the parameter range studied.

- The beryllium flux to remote areas results from effective reflection at the tungsten divertor tiles. However, with exposure time and thus beryllium deposition on the tiles beryllium reflection will be reduced but at the same time re-eroded beryllium will also contribute to the remote fluxes.
- The remote area below tile 5 is only accessible by neutral particles, whereas the inner louvre region can be also reached by ions.
- The impurity flux to remote areas strongly depends on the inner strike point position. Fluxes to the remote area below tile 5 are maximal when the strike point is located on the vertical tile 3 whereas fluxes to the inner louvre region are maximal when the strike point is on the horizontal tile 4, in particular at the sloping part of this tile.

If the same impurity influx (beryllium respectively carbon, relative to deuterium ion flux) into the inner divertor is assumed for JET-ILW and JET-C, the modelling leads to similar fluxes of carbon (JET-C) and beryllium (JET-ILW) to the remote area below tile 5. However, measurements of impurity deposition on the rotating collector probe below tile 5 from JET-ILW operation indicate about 10 times reduced beryllium deposition rate compared to carbon in JET-C. From this it can be concluded, that the beryllium influx into the inner divertor of JET-C is significantly smaller (factor 5 – 10) than the according carbon influx under JET-C operation. This is (qualitatively) supported by various observations like light emission within the inner divertor and also estimations of the main wall erosion source. Assuming such reduced beryllium flux in the order of 0.1% results in modelled beryllium deposition rates, which are in the same order of magnitude than the measured ones.

The simulations described in the present paper provide a more qualitative picture of the impurity transport to the remote areas of the inner divertor of JET. In the future further modelling is foreseen with the aim of a more quantitative comparison with experimental results. For this it would be very favourable to have shot-resolved deposition measurements with the QMB systems. This would enable more detailed parametric studies to analyse the influence of e.g. plasma parameters or strike point position on the deposition at remote areas, where the present modelling predicts clear tendencies. Also it could be studied whether an enhanced deposition within the inner louvre region occurs during ELMs as observed in JET-C [26]. Another open question is for instance whether net erosion at remote areas, as observed for JET-C for certain conditions, can also occur for JET-ILW.

To improve the assumption of beryllium flux into the divertor, the ERO modelling could be coupled with other simulations, which consider global transport and main wall erosion, see e.g. [26]. In addition, first attempts to simulate the beryllium transport from the main wall into the divertor with the ERO code are presented in [27].

ACKNOWLEDGEMENTS

This work was supported by EURATOM and carried out within the framework of the European Fusion Development Agreement. The views and opinions expressed herein do not necessarily reflect those of the European Commission. This work has been supported by the Sino-German Center for Research Promotion under Contract No. GZ769.

REFERENCES

[1]. J. Roth et al., Plasma Physics and Controlled Fusion **50** (2008) 103001

[2]. A. Kirschner et al., Physica Scripta **T138** (2009) 014011

[3]. G.F. Matthews et al., Journal of Nuclear Materials **438** (2013) S2

[4]. S. Brezinsek et al., Nuclear Fusion **53** (2013) 083023

[5]. A. Kirschner et al., Nuclear Fusion **40**, No.5 (2000) 989

[6]. S. Brezinsek et al., Journal of Nuclear Materials **438** (2013) S303

[7]. W. Eckstein, Computer simulation of ion-solid interaction, Springer Verlag, Berlin, 1991

[8]. D. Borodin et al., Physica Scripta **T159** (2014) 014057

[9]. K. Schmid et al., Nuclear Fusion **50** (2010) 105004

[10]. G. Kawamura et al., Journal of Nuclear Materials **438** (2013) S909

[11]. M.W. Thompson, Philos. Mag. **18** (1968) 377

[12]. J. Likonen et al., Physica Scripta **T159** (2014) 014016

[13]. A. Kreter et al., Plasma Phys. Control. Fusion **50** (2008) 095009

[14]. K. Krieger et al., Journal of Nuclear Materials **390–391** (2009) 110

[15]. T. Eich et al., Journal of Nuclear Materials **438** (2013) S72

[16]. G.J. van Rooij et al., Journal of Nuclear Materials **438** (2013) S42

[17]. H.G. Esser et al., Journal of Nuclear Materials **337–339** (2005) 84

[18]. H.G. Esser et al., Journal of Nuclear Materials **390–391** (2009) 148

[19]. A. Kirschner et al., Journal of Nuclear Materials **337–339** (2005) 17

[20]. A. Kirschner et al., Plasma and Fusion Research **8** (2013) 2402038

[21]. A. Widdowson et al., Physica Scripta **T159** (2014) 014010

[22]. J. Beal et al., these proceedings

[23]. D. Matveev et al., Plasma Physics and Controlled Fusion **52** (2010) 075007

[24]. J.P. Coad et al., Physica Scripta **T138** (2009) 014023

[25]. K. Schmid et al., these proceedings

[26]. A. Kreter et al., Physical Review Letters **102** (2009) 045007

[27]. M. Airila et al., these proceedings

	Measured deposition rate [particles/(cm^{2}s)]	**Modelled deposition rate [particles/(cm^{2}s)]**
Be	2e13 – 8e13	4e14 – 2e15 (L-Mode) 5e14 – 3e15 (H-Mode)
W	~ 5e11	5e9 – 8e11 (L-Mode) 5e11 – 5e13 (H-Mode)

Table 1: Measured and modelled beryllium and tungsten deposition rates on the rotating collector probe below tile 5 in JET-ILW. A beryllium influx to the inner divertor of 1% (relative to the deuterium ion flux) is assumed. The lower modelled values correspond to strike point on tile 4 and the upper ones for strike point on tile 3.

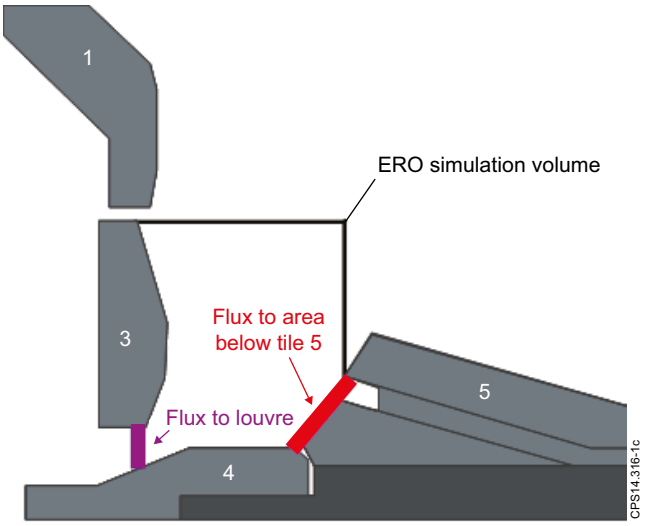

Figure 1: ERO simulation volume including the boundary surfaces for calculating the remote particle fluxes to the inner louvre and the region below tile 5.

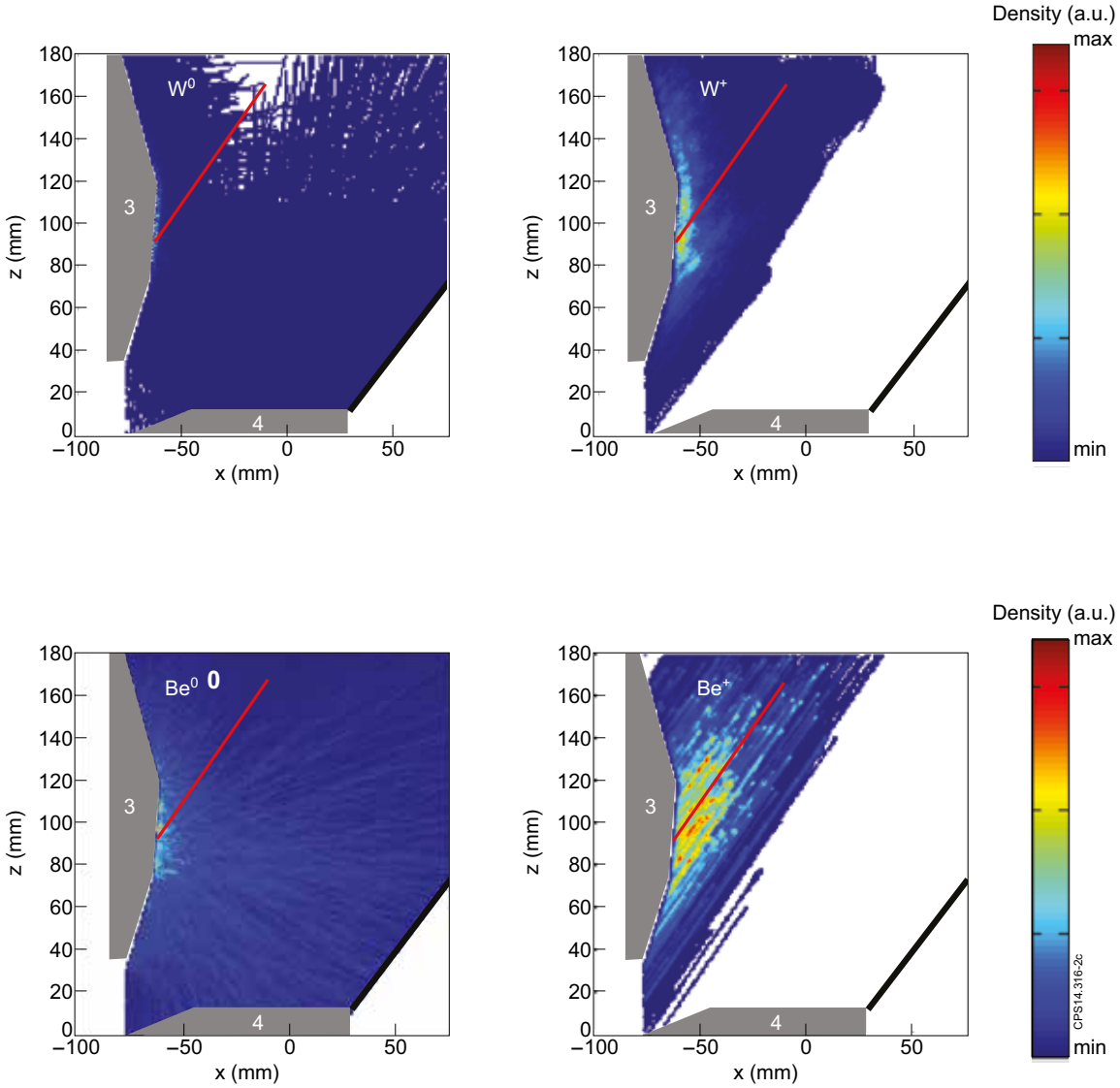

Figure 2: Modelled spatial distribution of sputtered tungsten (W^0 and W^+) and reflected beryllium (Be^0 and Be^+) within the inner divertor of JET-ILW for L-Mode condition and strike point located on tile 3.

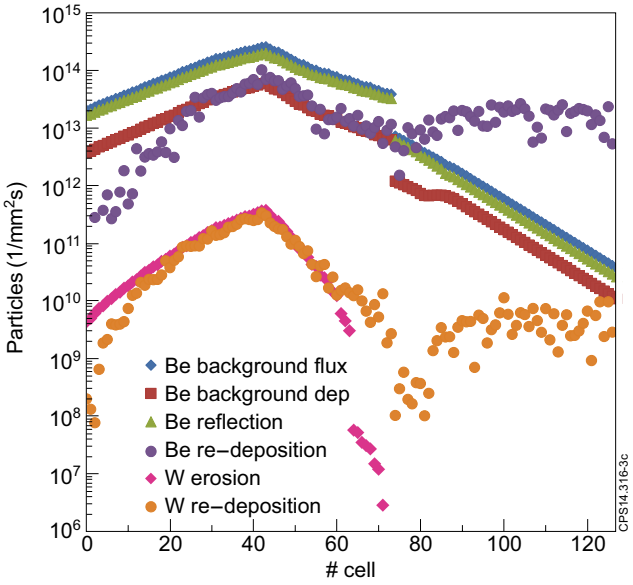

Figure 3: Modelled profiles of beryllium background flux, deposition of beryllium background flux, reflected beryllium, re-deposition of reflected beryllium, sputtered tungsten and re-deposition of sputtered tungsten along the inner divertor tiles of JET-ILW for L-Mode condition and the strike point located on tile 3. The numbering of the surface cells starts at the top of tile 3.

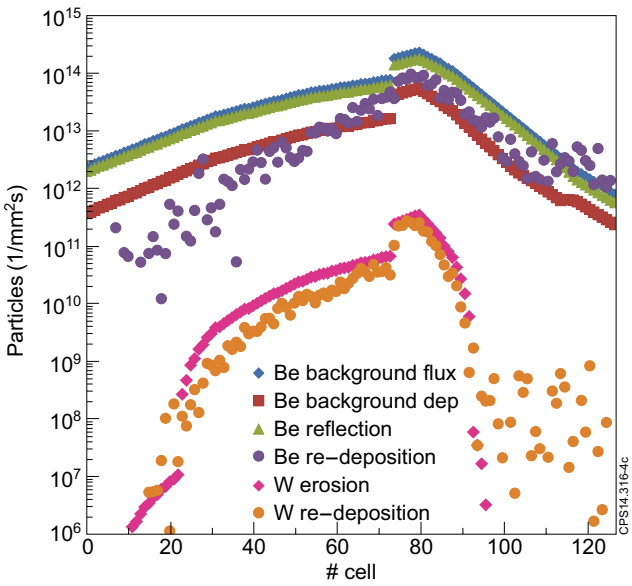

Figure 4: Modelled profiles of beryllium background flux, deposition of beryllium background flux, reflected beryllium, re-deposition of reflected beryllium, sputtered tungsten and re-deposition of sputtered tungsten along the inner divertor tiles of JET-ILW for L-Mode condition and the strike point located on tile 3. The numbering of the surface cells starts at the top of tile 4.

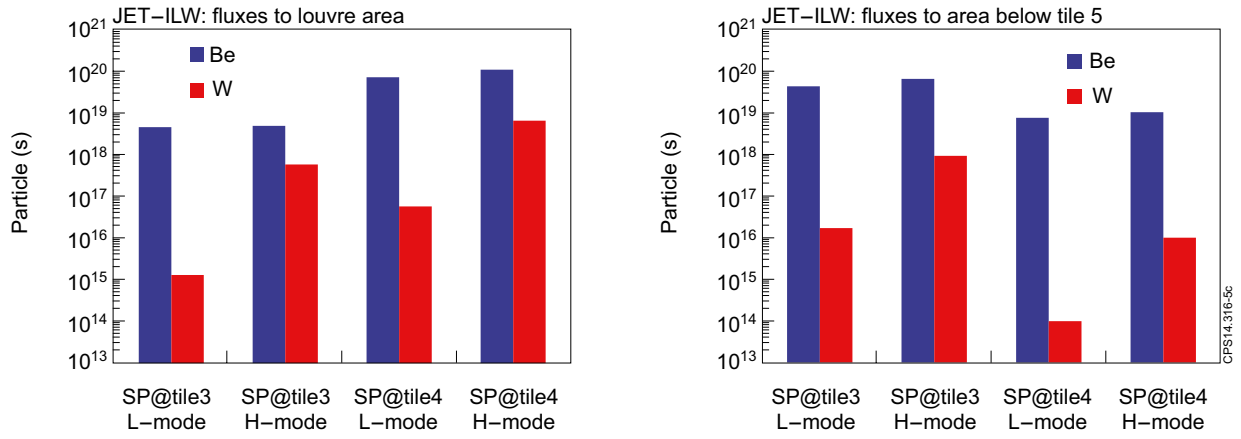

Figure 5: Modelled fluxes to the remote regions of JET-ILW. A beryllium influx to the inner divertor of 1% (relative to the deuterium ion flux) is assumed.

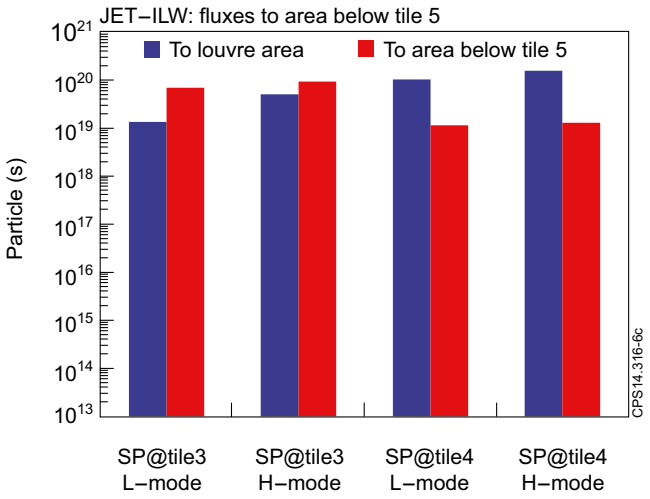

Figure 6: Modelled fluxes to the remote regions of JET-C. A carbon influx to the inner divertor of 1% (relative to the deuterium ion flux) is assumed.